Journal of Inorganic Biochemistry 227 (2022) 111667

Contents lists available at ScienceDirect

Journal of Inorganic Biochemistry

journal homepage: www.elsevier.com/locate/jinorgbio

# Screening the biological properties of transition metal carbamates reveals gold(I) and silver(I) complexes as potent cytotoxic and antimicrobial agents

Giulio Bresciani [a], Natalia Busto [b,*], Valentina Ceccherini [a], Marco Bortoluzzi [c], Guido Pampaloni [a,*], Begoña Garcia [b], Fabio Marchetti [a,*]

[a] University of Pisa, Department of Chemistry and Industrial Chemistry, Via G. Moruzzi 13, I-56124 Pisa, Italy
[b] University of Burgos, Department of Chemistry, Plaza Misael Bañuelos s/n, 09001 Burgos, Spain
[c] University of Venezia "Ca' Foscari", Department of Molecular Science and Nanosystems, Via Torino 155, I-30170 Mestre (VE), Italy

ARTICLE INFO

*Keywords:*
Metals in medicine
Anticancer metal complexes
Transition metal complexes
Metal carbamates
Cytotoxicity
Antibacterial activity

ABSTRACT

We report a screening study aimed to assess for the first time the air- and water-stability and the biological potential of simple metal-carbamates. These molecular metallic species are based on elements belonging to the groups 4–5, 7–9 and 11, and tin, and are easily available from inexpensive reagents. Complexes $[Ag(O_2CNEt_2)]$ (**13-Ag**) and $[Au(O_2CNMe_2)(PPh_3)]$ (**14-Au**) resulted substantially stable in aqueous media and exhibited a potent in vitro cytotoxicity. Especially **13-Ag** revealed a significant selectivity against the A549 lung adenocarcinoma and the A2780 ovarian cancer cell lines with respect to the noncancerous HEK293 cell line. Generation of ROS (reactive oxygen species) and mitochondrial membrane depolarization were recognized for **13-Ag** and **14-Au**; notwithstanding, the cell death mechanism is different in the two cases: apoptosis and cell cycle arrest in G0/G1 phase for **13-Ag**; necroptosis and cell cycle arrest in S phase for **14-Au**. Both **13-Ag** and **14-Au** are endowed with antibacterial activity, which is relatively stronger for **13-Ag** towards Gram negative and for **14-Au** towards Gram positive strains, respectively.

## 1. Introduction

Cancer is a public health problem and is one of the main causes of death worldwide [1]. Few platinum(II) complexes have been efficaciously administered against various types of tumors in admixture with other pharmaceuticals. Notwithstanding, the former are associated with some significant drawbacks such as severe side effects, acquired resistance phenomena and necessity of hospitalization for treatment [2]. Therefore, many efforts have been devoted to develop new anticancer metal drugs [3]. Indeed, transition metals possess peculiar properties not usually available on organic molecules and providing an enhanced potential in terms of antitumoral activity, such as the wide options of coordination environments and geometries, ligand activation and/or dissociation, and redox chemistry [4].

Many compounds based on transition metals have been explored as anticancer drug candidates, and a diversity of specific combinations of metals and ligands has revealed promising [3,4]. Homoleptic metal N,N-dialkylcarbamates constitute a large family of molecular compounds of formula $[M(O_2CNR_2)_n]_m$ (M = metal, R = alkyl group), which are accessible by means of the straightforward reaction between the metal chloride and an amine under $CO_2$ atmosphere at room temperature (Eq. (1)) [5].

$$MCl_n + n\,CO_2 + 2n\,NHR_2 \rightarrow \left[M(O_2CNR_2)_n\right] + n\,(NH_2R_2)Cl \quad (1)$$

Diverse synthetic procedures are also effective to obtain heteroleptic species comprising co-ligands [6]. Due to the simplicity and broad scope of the preparative methods, metal-carbamates have been reported for almost all the transition metals and also for some main-group elements bearing a metallic character [5]. Several carbamates of different metals behave as effective catalytic precursors in organic syntheses including carbon dioxide fixation under mild conditions [7], and also in hydrogenation reactions [8].

The monoanionic carbamato ligand may act as monodentate, chelating or bridging, adjusting its coordination to the environment, and it is usually reactive towards electrophiles. In particular, the interaction with protic species, including water, may lead to ligand decomposition with the release of amine and $CO_2$ and formation of metal oxide/hydroxide (Eq. (2)); this degradation occurs fast especially from

* Corresponding authors.
*E-mail addresses:* nbusto@ubu.es (N. Busto), guido.pampaloni@unipi.it (G. Pampaloni), fabio.marchetti1974@unipi.it (F. Marchetti).

https://doi.org/10.1016/j.jinorgbio.2021.111667
Received 26 August 2021; Received in revised form 14 November 2021; Accepted 14 November 2021
Available online 18 November 2021

carbamates of high valent, oxophilic metals [5a]. Accordingly, metal-carbamates have been traditionally handled and stored under inert (anhydrous) atmosphere to prevent contact with moisture, thus discouraging the investigation of possible biological applications.

$$\left[\{M\}(O_2CNR_2)_n\right] + n\ H_2O \rightarrow \left[\{M\}(OH)_n\right] + n\ CO_2 + n\ NHR_2 \quad (2)$$

Nevertheless, some platinum(IV) complexes (including mixed Ru—Pt compounds) containing an axial carbamato ligand have been recently considered as possible anticancer drugs, showing a substantial aqueous stability and an interesting cytotoxicity profile; the carbamate is released breaking up into carbon dioxide and amine following activation of the drug by metal reduction inside the cell [9]. This convenient strategy enables the delivery of bioactive amines to cancer cells [10]. Note that the performance offered by Pt-carbamato complexes is superior to that provided by homologous carboxylato species [11].

In the light of these results, and on account of the medicinal implications of organic carbamates [12], we became interested in evaluating the suitability of metal-carbamates to biological applications and, eventually, measuring their antiproliferative activity.

The structures of the molecules selected for the present study are drawn in Fig. 1. Some comments are required to justify the selection, in relation to analogous compounds with a documented history of anticancer studies. Titanocene dichloride, $[TiCp_2Cl_2]$, aroused much attention in the past, and entered clinical trials which were not finally successful [13]; the fast hydrolysis of the ligands in the physiological environment leads to the formation of Ti—O polymetallic derivatives, which are supposed to behave as the active species [14]. In principle, the titanium(IV) $[Ti(O_2CNEt_2)_4]$ (**1-Ti**) and the titanium(III) $[TiCp_2(O_2CNEt_2)]$ (**2-Ti**) represent alternative sources for such polymetallic species.

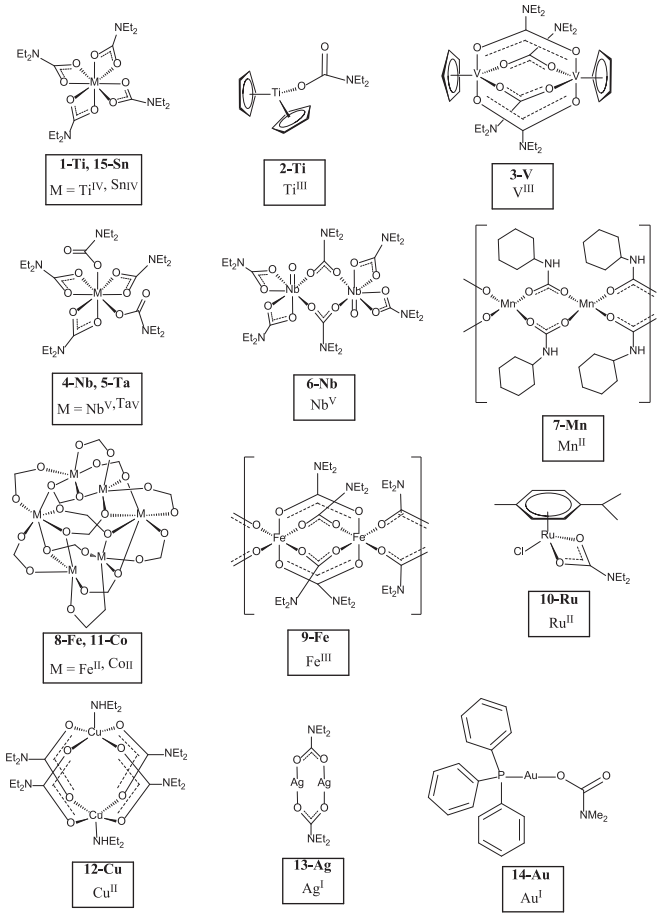


**Fig. 1.** Structures of metal-carbamates investigated in this work and related oxidation states of the metal centers.

Besides, vanadocene dichloride $[VCp_2Cl_2]$ possesses antitumor properties which have been the subject of studies even recently [15], and $[VCp_2(OH)_2]$ was detected as a probable key product of hydrolysis [16]. The replacement of the chloride ligands may be a key to the optimization of the anticancer behavior (see **3-V** as a new candidate) [17], and in particular vanadocene dithiocarbamates exhibited a strong cytotoxicity against leukemia cells [18]. Polymetallic oxido-hydroxido species are generally expected to form from niobium and tantalum precursors (see **4-Nb**, **5-Ta**, **6-Nb**), due to the strong oxophilicity of these metal centers [19], and niobium compounds of such type have revealed some anticancer potential [20]. Manganese (see **7-Mn**) is an element with several adjacent oxidation states, and this feature may favor the ROS-triggering activity of Mn coordination complexes, as recently demonstrated (ROS = reactive oxygen species) [21]. A variety of coordination complexes of iron(III) and iron(II) has been investigated for the antiproliferative activity, which is often associated with the redox chemistry of the iron, triggering the production of reactive oxygen species (see the $Fe^{II}$ and $Fe^{III}$ carbamates **8-Fe** and **9-Fe**) [22]. Complex **10-Ru** belongs to the widely investigated family of ruthenium(II) arene compounds [23], and it should be noted that arene-carboxylato complexes exert a cytotoxic effect despite the fast release of the carboxylate in aqueous media [24]. Sadler and co-workers studied the behavior of $[Ru(\kappa^2O\text{-}O_2CMe)Cl(p\text{-cymene})]$ in water and found that this compound converted into the hydroxo-bridged dimer $[\{Ru(p\text{-cymene})\}_2(\mu\text{-}OH)_3]^+$ [25]. In the framework of the intense research on gold(I) anticancer drugs [26], several studies on the cytotoxic activity of $[AuCl(PPh_3)]$ [27] and, more in general, of gold(I)-phosphine complexes have been reported (**14-Au** is unprecedented in this field) [28]. Cobalt [29], copper [30], silver [31] and tin [32] have also aroused attention for their possible antitumor activities in various forms (see the new candidates **11-Co**, **12-Cu**, **13-Ag** and **15-Sn**).

## 2. Results and discussion

### 1) Stability studies

Compounds shown in Fig. 1 were prepared by means of previously reported synthetic procedures (see Experimental). First, we monitored by IR spectroscopy (ATR reflectance method) the behavior of the carbamato complexes in contact with air: thus, complexes as powders were exposed to air in the absence of any matrix (e.g., Nujol or other) and related IR spectra were registered immediately after air contact and then at regular intervals of time. The main findings are compiled in Table 1, and views of the spectra are provided as Supporting Information. We found that IR spectra of **1-Ti**, **3-V**, **7-Mn**, **9-Fe**, **10-Ru**, **12-Cu**, **13-Ag**, **14-Au**, **15-Sn** did not change over 48 h. Conversely, decomposition was recognized for the remaining compounds, in some cases leading to derivatives still containing one or more carbamato units. In particular, the spectrum of **4-Nb** after 24 h indicated the disappearance of the band due to the monodentate carbamates (at ca. 1670 $cm^{-1}$), replaced by a new band ascribable to bridging carbamate(s) (at ca. 1580 $cm^{-1}$); this spectrum is almost superimposable to that of **6-Nb**, suggesting the prevalent conversion of $[Nb(O_2CNEt_2)_5]$ into $[NbO(O_2CNEt_2)_3]$. An analogous change was detected for **5-Ta** [33]. By comparison of the corresponding spectra, it is possible to assume the prevalent transformation of **8-Fe** into **9-Fe** after 24 h upon air contact, via clean $Fe^{II}$ to $Fe^{III}$ oxidation according to Belli and co-workers [34].

Based on the IR findings and with a view to the biological studies, we moved to assess the behavior in aqueous solution of those diamagnetic complexes exhibiting air stability, i.e. **1-Ti**, **10-Ru**, **13-Ag**, **14-Au** and **15-Sn**. Being insoluble in water, these complexes were dissolved in a DMSO-$d_6$/$D_2O$ mixture (DMSO = dimethylsulfoxide), and the resulting solutions were monitored by NMR spectroscopy (see Experimental for details). The dissociation of the carbamato ligands from the respective metal centers was ascertained along 24 h, resulting in the elimination of carbon dioxide and amine (see Eq. (2)), the latter detected as ammonium

**Table 1**
Overview of IR studies to check the inertness of metal-carbamates (solid-state) in air.

| Compound | Air inertness | Comments |
|---|---|---|
| $[Ti(O_2CNEt_2)_4]$ (**1-Ti**) | ≥ 48 h | |
| $[TiCp_2(O_2CNEt_2)]$ (**2-Ti**) | 1 h | Hydrolysis of Cp ligands. Partial hydrolysis of carbamate |
| $[V_2Cp_2(O_2CNEt_2)_4]$ (**3-V**) | ≥ 48 h | |
| $[Nb(O_2CNEt_2)_5]$ (**4-Nb**) | < 15 min | Hydrolysis of monodentate carbamates and formation of bridging carbamates. Formation of polynuclear oxido-carbamato species |
| $[Ta(O_2CNEt_2)_5]$ (**5-Ta**) | < 15 min | Partial hydrolysis of carbamates and formation of bridging carbamates. Formation of polynuclear oxido-carbamato species |
| $[NbO(O_2CNEt_2)_3]$ (**6-Nb**) | < 15 min | Partial hydrolysis of carbamates. Formation of polynuclear oxido-carbamato species |
| $[Mn(O_2CNHCy)_2]$ (**7-Mn**) | ≥ 48 h | |
| $[Fe(O_2CNEt_2)_2]$ (**8-Fe**) | 2 h | Prevalent conversion to **9-Fe** |
| $[Fe(O_2CNEt_2)_3]$ (**9-Fe**) | ≥ 48 h | |
| $[Ru(O_2CNEt_2)Cl(p\text{-cymene})]$ (**10-Ru**) | ≥ 48 h | |
| $[Co(O_2CNEt_2)_2]$ (**11-Co**) | 6 h | Hydrolysis |
| $[Cu(O_2CNEt_2)_2{\bullet}NHEt_2]$ (**12-Cu**) | ≥ 48 h | |
| $[Ag(O_2CNEt_2)]$ (**13-Ag**) | ≥ 48 h | |
| $[Au(O_2CNMe_2)(PPh_3)]$ (**14-Au**) | ≥ 48 h | |
| $[Sn(O_2CNEt_2)_4]$ (**15-Sn**) | ≥ 48 h | |

cation. This process is fast and complete in the cases of **10-Ru**, **15-Sn**, and **1-Ti**. The behavior of **10-Ru** in aqueous medium is in alignment with that of related ruthenium(II) carboxylato complexes, with the $^1$H NMR spectrum evidencing also partial dissociation of the *p*-cymene ring [35].

Remarkably, complexes **13-Ag** and **14-Au** revealed quite robust in the aqueous environment: the $^1$H NMR spectrum of **13-Ag** in DMSO-$d_6$/$D_2O$ did not change after 24 h at 37 °C, while only traces of dimethylamine were produced from **14-Au** under the same conditions. Consistently, $^{31}$P NMR spectroscopy on **14-Au** pointed out the presence of the starting compound and a secondary, minor species. A similar behavior was observed for **13-Ag** and **14-Au** in DMSO-$d_6$/phosphate buffer solution (pH = 7.4) at 37 °C. The speciation in DMSO/water of the paramagnetic compounds **3-V**, **7-Mn** and **9-Fe** was attempted based on mass spectrometry, but these experiments did not provide conclusive information; nevertheless, the detection of significant amounts of the amine is clearly ascribable to extensive ligand decomposition.

Furthermore, **13-Ag** and **14-Au** were NMR investigated for their stability in DMSO-$d_6$/DMEM cell culture mixture at 37 °C (DMEM = Dulbecco's Modified Eagle Medium). The robustness of **13-Ag** was confirmed, and after 24 h a small fraction (< 15%) of decomposition was detected. Instead, approximately 40% of **14-Au** was recovered after 24 h.

Overall, spectroscopic data indicate that a range of carbamato complexes are inert solid materials when stored in air, while in aqueous media they behave as precursors of various derivatives not easy to identify. In this setting, silver and gold complexes, **13-Ag** and **14-Au**, are exceptionally robust in aqueous solutions. In order to investigate this point more deeply, we carried out a DFT study. More precisely, we evaluated the Gibbs free energy for the hydrolysis of one carbamato ligand within complexes **1-Ti**, **3-V**, **13-Ag** and **14-Au**. The results are visualized in Eqs. (3)–(6). They evidence the tendency of the high valent, oxophilic titanium(IV) center in **Ti-1** to undergo degradation of the carbamate and its replacement with a hydroxide group; conversely, the softer V(III) derivative **3-V** and the late transition metal compounds **13-Ag** and **14-Au** appear rather stable towards the same reaction. According to this set of data, it is presumable that the partial decomposition detected for the latter complexes is followed by further structural rearrangement, possibly involving DMSO, and thus (slightly) shifting the equilibria of hydrolysis to the right.

$$\left[Ti(O_2CNEt_2)_4\right] + H_2O \rightarrow \left[Ti(OH)(O_2CNEt_2)_3\right] + NHEt_2 + CO_2 \quad (3)$$

$$\Delta G = -0.4\ \text{kcal}\cdot\text{mol}^{-1}$$

$$\left[V_2Cp_2(O_2CNEt_2)_4\right] + H_2O \rightarrow \left[V_2Cp_2(OH)(O_2CNEt_2)_3\right] + NHEt_2 + CO_2 \quad (4)$$

$$\Delta G = 8.9\ \text{kcal}\cdot\text{mol}^{-1}$$

$$[Au(O_2CNMe_2)(PPh_3)] + H_2O \rightarrow [Au(OH)(PPh_3)] + NHMe_2 + CO_2 \quad (5)$$

$$\Delta G = 12.7\ \text{kcal}\cdot\text{mol}^{-1}$$

$$\left[Ag_2(O_2CNEt_2)_2\right] + H_2O \rightarrow [Ag_2(OH)(O_2CNEt_2)] + NHEt_2 + CO_2 \quad (6)$$

$$\Delta G = 25.7\ \text{kcal}\cdot\text{mol}^{-1}$$

### 2) Cytotoxicity

The cytotoxic activity of the complexes was measured on the A549 and A2780 cancer cell lines following 24 h incubation, and on the nontumoral HEK293 cell line to outline a possible selectivity (Table 2). Cisplatin (**CDDP**), $AgNO_3$ and [Au(*Cl*)$PPh_3$] were analyzed as references. The carbamato complexes resulted inactive against the investigated cell lines, except **3-V**, **13-Ag** and **14-Au**. Vanadocene biscarbamate exhibits a moderate cytotoxicity, and it is noteworthy that $IC_{50}$ values on A549 cells are averagely lower than those obtained with other vanadocene derivatives bearing bidentate nitrogen ligands (48 h incubation) [36]. Complexes **13-Ag** and **14-Au** display a potent cytotoxicity especially against the A2780 cell line (micromolar range), and the antiproliferative effect is considerably higher than that of the reference compounds under the same conditions. Moreover, **13-Ag**, when compared to silver nitrate, is substantially more selective against the cancer cell lines with respect to the noncancerous cell lines [selectivity ratio SI = $IC_{50}$(HEK293) / $IC_{50}$(A2780)], highlighting that the activity of the silver carbamate cannot be merely attributed to the metal

**Table 2**
$IC_{50}$ values (μM) determined for carbamato complexes and cisplatin on human lung carcinoma (A549), human ovarian carcinoma (A2780) and healthy human embryonic kidney (HEK293) cells after 24 h incubation. Values are given as the mean ± SD. The $IC_{50}$ values of the corresponding best performers' metal salts ($AgNO_3$ and Cl-Au-$PPh_3$) were included for comparison purposes.

| Compound | A549 | A2780 | HEK293 |
|---|---|---|---|
| **1-Ti** | > 100 | > 100 | > 100 |
| **2-Ti** | > 100 | > 100 | > 100 |
| **3-V** | 49 ± 4 | 44.0 ± 1.6 | 74 ± 6 |
| **4-Nb** | > 100 | > 100 | > 100 |
| **5-Ta** | > 100 | > 100 | > 100 |
| **6-Nb** | > 100 | > 100 | > 100 |
| **7-Mn** | > 100 | > 100 | > 100 |
| **8-Fe** | > 100 | > 100 | > 100 |
| **9-Fe** | > 100 | > 100 | > 100 |
| **10-Ru** | > 100 | > 100 | > 100 |
| **11-Co** | > 100 | > 100 | > 100 |
| **12-Cu** | > 100 | > 100 | > 100 |
| **13-Ag** | 16 ± 2 | 0.4 ± 0.1 | 14 ± 2 |
| **14-Au** | 5.4 ± 0.7 | 0.9 ± 0.1 | 3.8 ± 0.4 |
| **15-Sn** | > 100 | > 100 | > 100 |
| **$AgNO_3$** | 33 ± 3 | 6.9 ± 0.9 | 7.5 ± 0.6 |
| **[AuCl($PPh_3$)]** | 18.6 ± 1.3 | 12.6 ± 1.4 | 15.4 ± 1.2 |
| **CDDP** | 40 ± 3 | 15.1 ± 1.2 | 65 ± 7 |

center, Fig. 2. The cytotoxicity exerted by **14-Au** appears comparable or even higher than that reported previously for other gold(I) triphenylphosphine complexes [37], including chloro(triphenylphosphine)gold (I) [38]. The selectivity of **14-Au** is comparable to that of cisplatin, while **3-V** is almost not selective (Fig. 2).

### 3) Mechanistic studies

We moved to perform targeted studies to elucidate the mechanism of action of the most promising compounds. It is documented that plasma protein binding controls the pharmacokinetics of drugs. Since albumin is the most abundant protein in plasma, the potential interaction of **13-Ag** and **14-Au** with BSA (bovine serum albumin) was evaluated by native polyacrylamide gel electrophoresis (Fig. S36). These experiments ruled out the occurrence of any binding. Hence, the accumulation of **13-Ag** and **14-Au** (and **CDDP** as reference) in A549, A2780 and HEK-293 cells was assessed by ICP-MS measurements, highlighting a relatively high level of internalization for both silver and gold species in the cancer cell lines (Fig. 3). Interestingly, **13-Ag** is significantly more internalized in A2780 than in HEK293 cell lines, and this fact has been correlated with the selectivity (see above).

Mitochondria constitute excellent targets for antitumor drug development, because their bioenergetics is essential to cancer metabolism and targeting mitochondria is also an efficient strategy to circumvent chemoresistance [39]. The anticancer action of several silver and gold complexes has been often related to this feature [31,40]. Since one manifestation of mitochondrial dysfunction is the decrease of the mitochondrial membrane potential (MMP), the effect of **13-Ag** and **14-Au** on the MMP was investigated by the use of TMRM (tetramethylrhodamine methyl ester): this molecular probe is internalized in active mitochondria and its fluorescence decreases on decreasing MMP [41]. After 1 h treatment of lung adenocarcinoma cells with either **13-Ag** or **14-Au**, MMP depolarization was observed, being more evident in cells incubated with **14-Au** than **13-Ag** (Fig. 4).

Mitochondrial dysfunction may lead to overproduction of reactive oxygen species (ROS), consequently to the disruption of the electron transport chain (ECT). Actually, mitochondria represent the main source of endogenous ROS, although ROS production may also arise from other enzymatic pathways (e.g., NADPH oxidases, xanthine oxidases, oxygenases) [42].

The ability of **13-Ag** and **14-Au** to induce ROS generation was investigated. ROS levels were assessed using the probe $H_2$DCFDA (dihydrodichlorofluorescein diacetate), which is internalized in the cells and hydrolyzed to dihydrodichlorofluorescein by esterases in the cytoplasm. The latter hydrolysis product can be readily oxidized by hydrogen peroxide, nitric oxide and peroxynitrite [43]. Both the analyzed metal-carbamates showed a significant ability to trigger ROS production in A549 cells (Fig. 5).

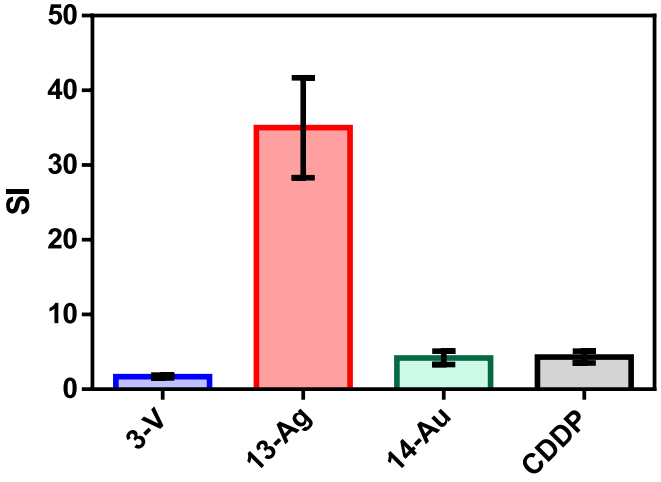


**Fig. 2.** Selectivity index (SI = $IC_{50}$(HEK293) / $IC_{50}$(A2780) ratio) of cytotoxic metal-carbamates and cisplatin.

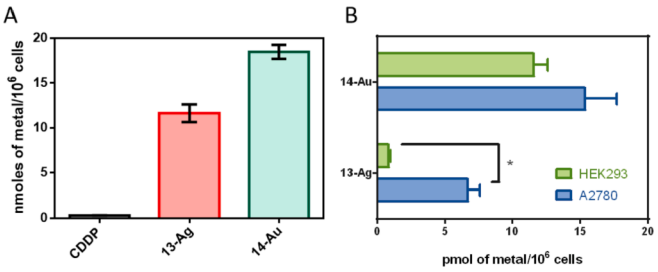


**Fig. 3.** A: Cellular uptake of **13-Ag**, **14-Au** and **CDDP** in A549 cells treated with 2 μM of the metal complexes. B: Cellular uptake of **13-Ag** and **14-Au** in A2780 and HEK293 cell lines after 24 h of treatment with 0.2 μM of the metal complexes. *Statistical significance, *p*-value <0.05 (ANNOVA).

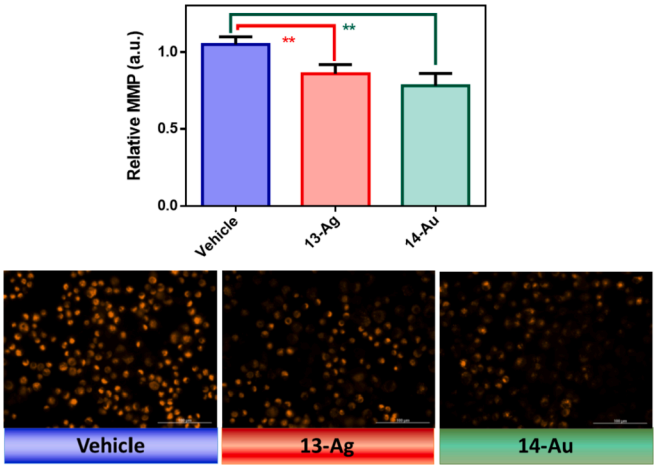


**Fig. 4.** Mitochondrial membrane potential measured by TMRM in A549 cells treated with the vehicle (0.5% DMSO) and the metal-carbamates at the respective $IC_{50}$ values. Results are expressed as the mean of relative emission (with respect to untreated cells) with standard deviation (SD). ** Statistical significance, *p*-value <0.01 (ANOVA-Dunnett).

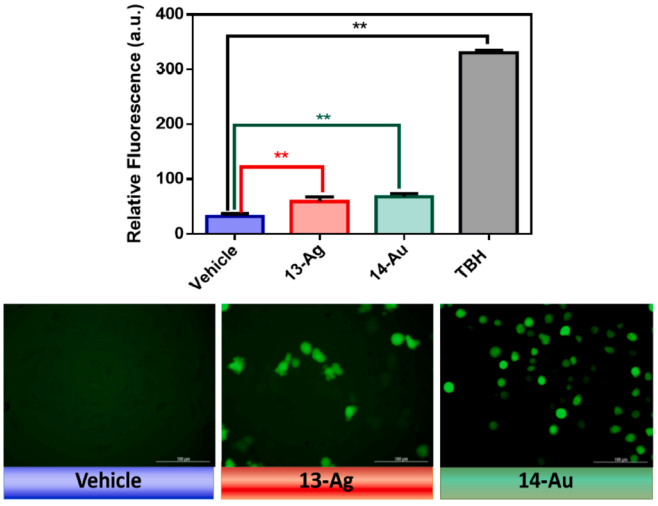


**Fig. 5.** Detection of ROS by $H_2$DCFDA in A549 cells after 4 h of treatment. Treatment with 10 μM tert-butyl-hydroperoxide, TBH, was included as positive control. Data are the mean of two different experiments ± SD. ** Statistical significance *p*-value <0.01 (ANOVA-Dunnett).

ROS generation was also investigated by means of the DHE (dihydroethidium) probe, aimed to detect the superoxide anion ($O_2^-$) [44]. Interestingly, **13-Ag** led to an increase of the superoxide level, conversely **14-Au** did not produce any appreciable effect (Fig. 6).

Our findings indicate that cytotoxic metal-carbamates may cause cell death via oxidative stress stimulation. In principle, there are different mechanisms for cell death linked to ROS generation [45]; in particular, MMP depolarization, as observed here, points out to programmed cell death via an intrinsic pathway. To confirm this hypothesis, apoptosis induction was studied by flow cytometry. Thus, **13-Ag** and **14-Au**, at the respective $IC_{50}$ values, induced apoptosis in A549 cells after 24 h of incubation, with a significant fraction of cells in late apoptosis and necrosis (Fig. 7). More precisely, treatment with **14-Au** led to almost 30% of necrotic cells, while following treatment with **13-Ag** the percentage of apoptotic cells resulted greater than that of necrotic ones. These outcomes demonstrate that cell death arises from different pathways promoted by **13-Ag** and **14-Au**, respectively.

Furthermore, cell cycle experiments over 24 h confirmed the different modes of action of the silver and gold complexes. In detail, **13-Ag** elicited accumulation of A549 cells in G0/G1 phase with a decrease in G2/M; by contrast, **14-Au** favored cell accumulation in S phase, analogously to cisplatin, and a marked decrease in G2/M (Fig. 8).

A considerable effort of research has been devoted to the development of silver complexes as suitable antimicrobial agents [40a,46], whereas related studies on gold complexes are more limited [47]. The antibacterial potential of **13-Ag** and **14-Au** was evaluated on four pathogenic bacteria of clinical interest, i.e. two Gram-positive (vancomycin-resistant *Enterococcus faecium* and methicillin–resistant *Staphylococcus aureus*) and two Gram negative (*Acinetobacter baumanii* and *Pseudomonas aeruginosa*) strains. The antibiotic norfloxacin, $AgNO_3$ and [$AuCl(PPh_3)$] were employed as references. The resulting minimal inhibitory concentrations (MIC) are compiled in Table 3. Briefly, both the analyzed carbamato complexes possess antibacterial properties. More precisely, **13-Ag** is more active towards Gram negative than Gram positive strains, while silver nitrate revealed a bactericidal potency which is almost the same in all the tested bacteria. Furthermore, **14-Au** showed the opposite trend with respect to **13-Ag**, and [$AuCl(PPh_3)$] is inactive towards the Gram negative strains.

## 3. Conclusions

Metal-carbamates are easily available coordination compounds known for most of the metal elements in the periodic table, and traditionally handled and stored under inert atmosphere due to their generally claimed sensitivity to water. Here, for the first time, we have tested the suitability to biological applications of a range of molecular metal-carbamates (both homo- and heteroleptic), including analogues of well-established anticancer metal structures, highlighting the substantial stability in air of a variety of complexes. NMR studies suggest the fast generation of polymetallic aggregates in aqueous solution, upon complete or partial release of the carbamato ligands. Otherwise, [Ag($O_2CNEt_2$)] (**13-Ag**) and [Au($O_2CNMe_2$)($PPh_3$)] (**14-Au**) emerged as exceptions for their stability in physiological media and potent cytotoxic activity against cancer cell lines, which is featured by a significant degree of selectivity (A2780 vs. HEK293 cells) in the case of the silver

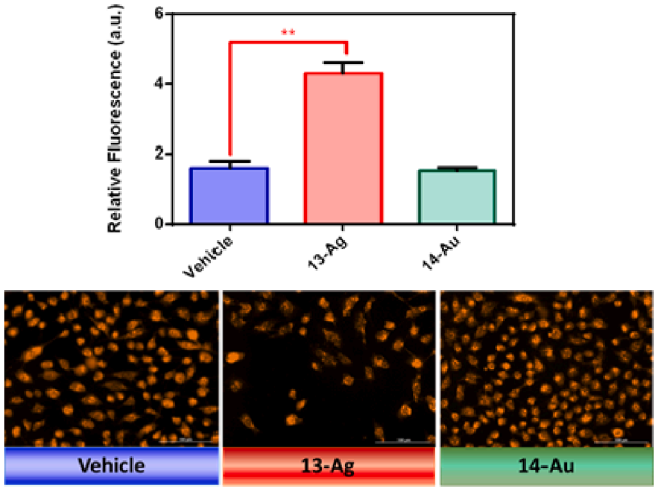


**Fig. 6.** Detection of superoxide anion by DHE in A549 cells after 2 h of treatment. Data are the mean of two independent experiments ± SD. ** Statistical significance p-value <0.01 (ANOVA-Dunnett).

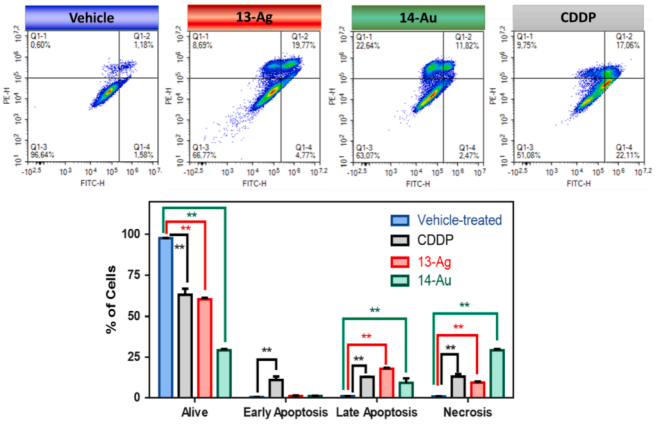


**Fig. 7.** Flow cytometry results of Annexin V-FITC/PI double staining of A549 cells treated with the metal complexes at the respective $IC_{50}$ values. Results are expressed as % of A549 cells in alive, early apoptotic, late apoptotic and necrotic phases. Data were obtained from duplicates of two different experiments and plots express mean values with standard deviation. ** Statistical significance, *p*-value <0.01 (ANOVA-Dunnett).

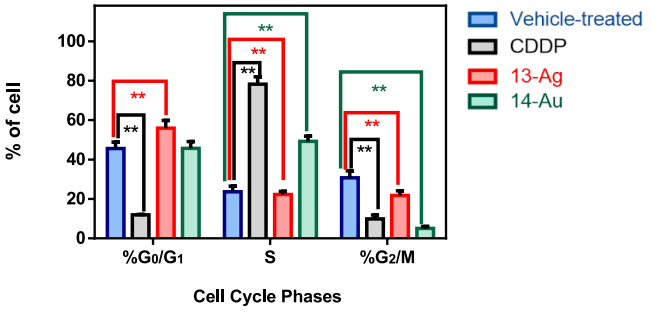


**Fig. 8.** Flow cytometer analysis of cell cycle distribution of A549 cells incubated for 24 h with selected metal-carbamates. Data were obtained from duplicates of two different experiments and plots express mean values with standard deviation. ** Statistical significance, p-value <0.01 (ANOVA-Dunnett).

**Table 3**
MIC values (= the lowest compound concentration preventing bacterial growth) obtained for silver and gold carbamates. $AgNO_3$, [$AuCl(PPh_3)$] and the antibiotic norfloxacin as references.

| | MIC (μM) | | | |
|---|---|---|---|---|
| Compound | *E. faecium* | *S. aureus* | A. baumanii | *P. aeruginosa* |
| **13-Ag** | 50 | 25 | 12.5 | 6.2 |
| **14-Au** | 5 | 3.1 | 25 | 25 |
| **$AgNO_3$** | 6.2 | 12.5 | 6.2 | 6.2 |
| **[$AuCl(PPh_3)$]** | 3.1 | 3.1 | 100 | >100 |
| **Norfloxacin** | 6.2 | 6.2 | 20 | 3.1 |

complex, according to a relatively higher degree of internalization in the tumor cell line. To best of our knowledge, **13-Ag** and **14-Au** represent the very first cases of group 11 metal complexes with a carbamato ligand ever investigated for biological purposes. Experiments reveal that the mode of action is ascribable essentially to redox unbalance inside the cells, however different pathways are viable for the two complexes. Additionally, **13-Ag** and **14-Au** possess specific bactericidal properties against Gram-positive and Gram-negative pathogens of clinical interest, outlining a potential development as combined antitumor and prophylactic chemotherapic agents.

## 4. Experimental

### 1) Materials and methods

Compounds $[Ti(O_2CNEt_2)_4]$ (**1-Ti**) [48], $[TiCp_2(O_2CNEt_2)]$ (**2-Ti**), $[V_2Cp_2(O_2CNEt_2)_4]$ (**3-V**) and $[M(O_2CNEt_2)_5]$ (M = Nb, **4-Nb**; M = Ta, **5-Ta**) [49], $[NbO(O_2CNEt_2)_3]$ (**6-Nb**) [33], $[Mn(O_2CNHCy)_2]$ (**7-Mn**) and $[Fe(O_2CNEt_2)_2]$ (**8-Fe**) [34], $[Fe(O_2CNEt_2)_3]$ (**9-Fe**) [50], $[Ru(O_2CNEt_2)Cl(p\text{-cymene})]$ (**10-Ru**) [51], $[Co(O_2CNEt_2)_2]$ (**11-Co**) [52], $[Cu(O_2CNEt_2)_2{\bullet}NHEt_2]$ (**12-Cu**) [53], $[Ag(O_2CNEt_2)]$ (**13-Ag**) [54], $[Au(O_2CNMe_2)(PPh_3)]$ (**14-Au**) [54] and $[Sn(O_2CNEt_2)_4]$ (**15-Sn**) [55] were prepared according to the respective literature procedures. IR spectra (650–4000 $cm^{-1}$) were recorded on a Perkin Elmer Spectrum One FT-IR spectrometer, equipped with a UATR sampling accessory. IR spectra were processed with Spectragryph software [56]. NMR spectra were recorded at 298 K with a Bruker Avance II DRX 400 instrument equipped with a BBFO broadband probe. Chemical shifts (expressed in parts per million) are referenced to the residual solvent peaks [57] ($^1H$, $^{13}C$) or to external standard ($^{31}P$ to 85% $H_3PO_4$) [58].

### 2) IR studies

*General procedure*. A sealed glass tube containing the selected compound (70 mg) under $N_2$ atmosphere was opened and the IR spectrum of the solid sample was immediately registered ($t = 0$). The solid was then allowed to contact with air for 15 min and subsequently analyzed by IR spectroscopy. IR analysis was repeated on the solid material, left in contact with air, after 1 h, 2 h, 6 h, 24 h, 48 h.

**$[Ti(O_2CNEt_2)_4]$, 1-Ti.** IR ($t = 0$, unchanged at $t = 48$ h): $\tilde{\upsilon}/cm^{-1}$ = 2975w, 2934w, 2875vw, 1550vs (CO), 1500vs, 1435s, 1377 m, 1314s, 1212 m, 1078 m, 978w, 939w, 838 s, 787 s.

**$[TiCp_2(O_2CNEt_2)]$, 2-Ti.** IR (t = 0): $\tilde{\upsilon}/cm^{-1}$ = 2966w, 2931w, 2871vw, 1714w (CO), 1618w, 1530s, 1490s, 1435s, 1323 m, 1262 m, 1192w, 1095 m, 1015 m. IR ($t = 24$ h, unchanged at $t = 48$ h): $\tilde{\upsilon}/cm^{-1}$ = 2968w, 2931w, 2871vw, 1744vw, 1708w, 1520 m, 1488s, 1434 m, 1377w,1309 m, 1213w, 1090w, 1073 m, 1016 m, 791vs.

**$[VCp_2(O_2CNEt_2)_4]$, 3-V.** IR ($t = 0$, unchanged at t = 48 h): $\tilde{\upsilon}/cm^{-1}$ = 2968w, 2925w, 2869vw, 1597s (CO), 1492vs, 1459 m, 1426s, 1374 m, 1317vs, 1220 m, 1089 m, 1017w, 978w, 787vs.

**$[Nb(O_2CNEt_2)_5]$, 4-Nb.** IR (t = 0): $\tilde{\upsilon}/cm^{-1}$ = 2973w, 2933w, 2875vw, 1676w (CO), 1560vs (CO), 1504 m, 1482 m, 1438s, 1378 m, 1313s, 1211 m, 1077 m, 974w, 931 m, 836 m, 782 s. IR ($t = 24$ h, unchanged at $t = 48$ h): $\tilde{\upsilon}/cm^{-1}$ = 2972w, 2934w, 2873vw, 1624 m, 1570s, 1560s, 1484s, 1435s, 1378 m, 1209 m, 1099w, 1076w, 979w, 930vs, 889w, 840 m, 782 m

**$[Ta(O_2CNEt_2)_5]$, 5-Ta.** IR ($t = 0$): $\tilde{\upsilon}/cm^{-1}$ = 2971w, 2934w, 2875vw, 1661 m (CO), 1601vs (CO), 1455 m, 1404 m, 1381w, 1325 m, 1261s, 1169 m, 1099w, 1059w, 964w, 874w, 843 m, 813 m, 778 s. IR ($t = 24$ h, unchanged at $t = 48$ h): $\tilde{\upsilon}/cm^{-1}$ = 2970w, 2933w, 2874vw, 1659 m, 1602vs, 1556 m, 1456 m, 1404 m, 1324 m, 1261vs, 1225w, 1212 m, 1190 m, 1168s, 1092 m, 964w, 937w, 843 m, 813 m, 777vs.

**$[NbO(O_2CNEt_2)_3]$, 6-Nb.** IR ($t = 0$): $\tilde{\upsilon}/cm^{-1}$ = 2967w, 2936w, 2875vw, 1621 m (CO), 1579vs (CO), 1558vs, 1484vs, 1434vs, 1379 m, 1303s, 1261 m, 1209 m, 1097 m, 1074 m, 1020 m, 930vs, 840 m, 796 s. IR (t = 24 h, unchanged at $t = 48$ h): $\tilde{\upsilon}/cm^{-1}$ = 2972w, 2933w, 2874vw, 1624 m, 1557s, 1530s, 1489vs, 1456s, 1433vs, 1378 m, 1319s, 1305s, 1208 m, 1074 m, 969 m, 928 s, 894 m, 839 m, 782 s, 734 s, 670 s.

**$[Mn(O_2CNHCy)_2]$, 7-Mn.** IR ($t = 0$, unchanged at $t = 48$ h): $\tilde{\upsilon}/cm^{-1}$ = 3317br (NH), 2925 m-s, 2852 m, 1558vs (CO), 1525vs, 1450 m, 1385 m, 1342s, 1289 m, 1259 m, 1045w, 803 m, 718w.

**$[Fe(O_2CNEt_2)_2]$, 8-Fe.** IR ($t = 0$): $\tilde{\upsilon}/cm^{-1}$ = 2974w, 2931w, 2871vw, 1590 m (CO), 1516s, 1482vs, 1423s, 1374 m, 1309vs, 1214 m, 1085 m, 975w, 935vw, 798 m-s, 776 m. IR (t = 24 h, unchanged at $t = 48$ h): $\tilde{\upsilon}/cm^{-1}$ = 2972w, 2930w, 2871vw, 2822vw, 1488vs, 1459 m, 1427s, 1375 m, 1309s, 1217 m, 1090 m, 1073 m, 977w, 937vw, 835vw, 797 m, 778 m 724w.

**$[Fe(O_2CNEt_2)_3]$, 9-Fe.** IR ($t = 0$, unchanged at $t = 48$ h): $\tilde{\upsilon}/cm^{-1}$ = 2974w, 2931w, 2869vw, 1488vs (CO), 1455 m, 1428s, 1374 m, 1309s, 1222 m, 1089 m, 972w, 939vw, 804 m, 784 m.

**$[Ru(O_2CNEt_2)Cl(p\text{-cymene})]$, 10-Ru.** IR ($t = 0$, unchanged at $t = 48$ h): $\tilde{\upsilon}/cm^{-1}$ = 3062w, 2965 m, 2931vw, 2871vw, 1548vs (CO), 1474s, 1444 m, 1376 m, 1337s, 1215w, 1054 m, 881w, 829 m.

**$[Co(O_2CNEt_2)_2]$, 11-Co.** IR (t = 0): $\tilde{\upsilon}/cm^{-1}$ = 2967w, 2931w, 2872vw, 1593 m (CO), 1520 m-s (CO), 1480vs, 1458 m, 1421vs, 1374 m, 1308vs, 1214 m, 1085 m, 975 m, 935w, 798 s, 778 m. IR (t = 48 h): $\tilde{\upsilon}/cm^{-1}$ = 2967w, 2930w, 2872vw, 1540 m, 1476s, 1416s, 1373 m, 1303vs, 1213w, 1138w, 1084w, 1068w, 975w, 935vw, 839 m, 800 m, 776 m, 755 m.

**$[Cu(O_2CNEt_2)_2{\bullet}NHEt_2]$, 12-Cu.** IR (t = 0, unchanged at t = 48 h): $\tilde{\upsilon}/cm^{-1}$ = 2967w, 2929w, 2871vw, 1594 m (CO), 1487vs, 1458 m, 1424vs, 1374 m, 1314vs, 1216 m, 1160w, 1089 m, 1031w, 975w, 933 m, 908w, 792 s.

**$[Ag(O_2CNEt_2)]$, 13-Ag.** IR (t = 0, unchanged at t = 48 h): $\tilde{\upsilon}/cm^{-1}$ = 2963w, 2927w, 2869vw, 1480 m (CO), 1413s, 1373 m, 1301 m, 1210w, 1082s, 975sh, 867 m,

**$[Au(O_2CNMe_2)(PPh_3)]$, 14-Au.** IR (t = 0, unchanged at t = 48 h): $\tilde{\upsilon}/cm^{-1}$ = 3064vw, 3047vw, 2962w, 2907w, 2843vw, 1604s (CO), 1570 m, 1480s, 1434vs, 1372vs, 1312w, 1225vs, 1182 m, 1158 m, 1026s, 997 m, 791 s, 746vs, 711 m, 692vs.

**$[Sn(O_2CNEt_2)_4]$, 15-Sn.** IR (t = 0, unchanged at t = 48 h): $\tilde{\upsilon}/cm^{-1}$ = 2963w, 293w, 2875vw, 1561s (CO), 1517s, 1439 m, 1383w, 1348w, 1317 m, 1210 m, 1076s, 1017s, 976 m, 939w, 853 m, 792vs.

### 3) NMR studies

a) *Stability in dmso-$d_6$/$D_2O$ solution.* Each diamagnetic compound (25 mg) was dissolved into DMSO-$d_6$ (0.45 mL), and the resulting solution was diluted with $D_2O$ (0.15 mL) in air. A carefully weighted amount of dimethylsulfone (ca 1.5 mg) was added as internal standard. The final mixture was analyzed by NMR spectroscopy at RT after being stored at 37 °C for 15 min and 24 h, respectively. No significant change in the spectra was observed after 24 h compared to the corresponding spectra after 15 min. Data related to either ammonium (from carbamato decomposition) or secondary metal species are italicized.

**$[Ti(O_2CNEt_2)_4]$, 1-Ti**. $^1H$ NMR ($CDCl_3$): $\delta$/ppm = 3.27 (q,$^3J_{HH}$ = 7.0 Hz, 2H, $CH_2$); 0.99 (t,$^3J_{HH}$ = 6.9 Hz, 3H, $CH_3$). $^1H$ NMR (DMSO-$d_6$ + $D_2O$): $\delta$/ppm = *4.32* (br, NH); *2.85* (br, 2H, $CH_2$); *1.11* (br, 3H, $CH_3$) [59].

**$[Ru(O_2CNEt_2)Cl(p\text{-cymene})]$, 10-Ru.** $^1H$ NMR ($C_6D_6$): $\delta$/ppm = 5.0, 4.7 (d,$^3J_{HH}$ = 6.0 Hz, 4H, arom CH); 3.0 (q, 4H, $NCH_2$); 2.7 (hept, 1H, *CH*$Me_2$); 1.9 (s, 3H, Me-cym); 1.1 (d, 6H, *CHMe*$_2$); 0.9 (t, 6H, $NCH_2$*Me*) [51]. $^1H$ NMR (DMSO-$d_6$ + $D_2O$): $\delta$/ppm = *7.05* (m, CH); 5.44, 5.23 (d,$^3J_{HH}$ = 5.8 Hz, arom CH); *4.20* (br, NH); *2.87* (q,$^3J_{HH}$ = 7.2 Hz, $NCH_2$); 2.75 (hept, *CH*$Me_2$); *2.18* (s, Me); 2.07 (s, Me-cym); 1.20 (d,$^3J_{HH}$ = 8.2 Hz, *CHMe*$_2$); *1.12* (m, $NCH_2$*Me*); *0.66* (d,$^3J_{HH}$ = 7.8 Hz, CH*Me*$_2$).

**$[Ag(O_2CNEt_2)]$, 13-Ag.** $^1H$ NMR ($C_6D_6$) [54]: $\delta$/ppm = 3.48 (q, 2H, $CH_2$); 1.22 (t, 3H, $CH_3$). $^1H$ NMR (DMSO-$d_6$ + $D_2O$): $\delta$/ppm = 2.55 (q,$^3J_{HH}$ = 7.3 Hz, 2H, $CH_2$); 1.02 (t,$^3J_{HH}$ = 7.0 Hz, 3H, $CH_3$).

**$[Au(O_2CNMe_2)(PPh_3)]$, 14-Au.** $^1H$ NMR (toluene-$d_8$): $\delta$/ppm = 7.02–6.87 (m, 15H, Ph); 3.11 (s, 6H, Me). $^{31}P\{^1H\}$ NMR (toluene-$d_8$):

$\delta$/ppm = 27.7. $^1$H NMR (DMSO-$d_6$ + $D_2O$): $\delta$/ppm = 7.53–7.11 (m, Ph); *4.21* (s, NH); 2.65, *2.55* (s, Me). $NHMe_2$ / $Me_2SO_2$ ratio = 0.5. $^{31}P\{^1H\}$ NMR (DMSO-$d_6$ + $D_2O$): $\delta$/ppm = *29.5*, 23.1 (ratio 1:2).

**[Sn($O_2CNEt_2$)$_4$] , 15-Sn.** $^1$H NMR ($CDCl_3$): $\delta$/ppm = 3.30 (q, $^3J_{HH}$ = 7.0 Hz, 2H, $CH_2$); 1.07 (t, $^3J_{HH}$ = 7.1 Hz, 3H, $CH_3$). $^1$H NMR (DMSO-$d_6$ + $D_2O$): $\delta$/ppm = *4.40* (br, NH); *2.83* (br, 2H, $CH_2$); *1.11* (br, 3H, Me).

b) *Stability in phosphate buffer solution.* The selected complex (**13-Ag** or **14-Au**, ca. 15 mg) was dissolved in DMSO-$d_6$ (0.45 mL), and the resulting solution was diluted with 0.15 mL of $NaH_2PO_4$ / $Na_2HPO_4$ solution in $D_2O$ (phosphate concentration 80 mM, pD = 7.4). A carefully weighted amount of dimethylsulfone (ca 1.5 mg) was added as internal standard. The final mixture was analyzed by $^1$H (and $^{31}$P NMR, in the case of **14-Au**) spectroscopy at RT, after being stored at 37 °C for 15 min and 24 h, respectively. The spectra of **14-Au** did contain the signal of the starting species only; the spectrum of **13-Ag** evidenced the formation of dimethylamine after 15 min (1:4 ratio with respect to **13-Ag**), and this ratio did not change after 24 h.

c) *Stability in the cell culture medium.* Powdered DMEM cell culture medium (1000 mg/L glucose and L-glutamine, without sodium bicarbonate and phenol red; D2902 - Merck) was dissolved in $D_2O$ (10 mg/mL), according to the manufacturer's instructions. The solution of deuterated cell culture medium ("DMEM-d") was treated with $Me_2SO_2$ (6.6 mM) and $NaH_2PO_4$ / $Na_2HPO_4$ (0.15 M, pD = 7.5 [60]), then stored at 4 °C under $N_2$. An aliquot of this mixture (0.10 mL) was added to a solution of the selected complex (**13-Ag** or **14-Au**, ca. 5 mg) in DMSO-$d_6$ (0.45 mL); the final solution was stored at 37 °C for 15 min and 24 h, respectively. NMR spectra after 15 min allowed to quantify the amount of residual compound as >85% (from **13-Ag**) and ~ 40% (from **14-Au**). No significant change was observed after 24 h.

### 4) Cytotoxicity

Human lung adenocarcinoma (A549), ovarian cancer (A2780) and embryonic kidney cells (HEK-293) were obtained from the European Collection of Cell Cultures (EACC). A549 cells were cultured in DMEM (Dulbecco's Modified Eagle Medium) and A2780 cells in RPMI-1640, supplemented with 2 mM of glutamine; HEK293 cells in MEM were supplemented with 2 mM of glutamine and 1% of nonessential amino acids (NEAA). All media were supplemented with 10% fetal bovine serum (FBS) and 1% amphotericin-penicillin-streptomycin solution. $IC_{50}$ values were determined by the MTT (3-(4,5-dimethyltiazol-2-yl)-2,5-diphenyltetrazoliumbromide) assay as previously described [61]. Briefly, cells were seeded in 96-well plates at a density of $5 \times 10^3$ (A549) or $1 \times 10^4$ (A2780 and HEK293) cells per well. After 24 h, cells were treated with different concentrations of the complexes and cisplatin as positive control. Since the metal-carbamates were dissolved in DMSO, a vehicle control with DMSO at the maximal employed concentration (0.5%) was also included. After 24 h of treatment, cells were incubated with the MTT solution (500 μg/mL) for 3 h. Afterwards, the formazan crystals were dissolved, and absorbance was read at 590 nm in a microplate reader (Cytation 5 Cell Imaging Multi-Mode Reader, Biotek Instruments, USA). Two independent experiments were performed with four replicates per dose. The $IC_{50}$ values were calculated using GraphPadPrism Software Inc. (version 6.01) (USA).

### 5) Cellular uptake

A549 cells ($1.5 \times 10^5$) were seeded in 2 mL of complete culture medium in 6-well plates and grown for 24 h at 37 °C and 5% $CO_2$. Cells were then treated with 2 μM of cisplatin, **13-Ag** and **14-Au**, respectively, for 24 h. A2780 and HEK293 cells ($5 \times 10^5$) were seeded and treatment was performed with 0.2 μM of **13-Ag** and **14-Au**. Afterwards, cells were washed for three times with DPBS (Dulbecco's Phosphate Buffered Saline) and harvested in 1 mL of DPBS. 10 μL of each sample were used to assess the number of cells in a TC20 automated cell counter (Biorad). Then, samples were digested with 65% $HNO_3$ and analyzed in a 8900 ICP-MS (Agilent Technologies). Data are reported as the mean and standard deviation of two independent experiments with two replicates.

### 6) Intracellular ROS generation

A549 cells were seeded in a clear bottom black side 96 well plate (Costar) at a density of $3 \times 10^4$ cells per well and incubated for 24 h. Then, for ROS quantification with the probe $H_2$DCFDA, 100 μL of 25 μM 2′-7′-dichlorofluorescein diacetate was added to each well. After 30 min of incubation, cells were treated with 100 μL of the appropriate complex at the same concentration as the $IC_{50}$ value. 20 μM of TBH was included as positive control. After 2 h of treatment, cells were washed twice with DPBS and emission was measured at $\lambda_{em}$ = 530 nm with $\lambda_{exc}$ = 490 nm during 2 h in a microplate reader (Cytation 5 Cell Imaging Multi-Mode Reader, Biotek Instruments, USA). Measurements at 3.5 h after treatment were selected at the final point for data analysis. Cell images were recorded, and the collected results were corrected by the number of cells obtained from an identical plate stained with 0.5 μM of Hoechst33250. Two independent experiments with four replicates per treatment were performed.

For ROS quantification with DHE, cells were incubated with 0.5 μM of DHE (dihydroethidium) for 20 min. Then, cells were washed twice with PBS and fluorescence intensity was measured after 2 h of treatment at $\lambda_{em}$ = 535 nm with $\lambda_{exc}$ = 635 nm in a microplate reader (Cytation 5 Cell Imaging Multi-Mode Reader, Biotek Instruments, USA). The emission of each well was corrected by the number of cells. Results are expressed as the mean and standard deviation of two independent experiments with 4 replicates per dose.

For MMP evaluation, A549 cells were seeded in a Costar clear bottom black side 96 well plate at a density of $3 \times 10^4$ cells per well. After 24 h of incubation, media was removed and replaced by 100 μL of assay buffer (25 mM D-glucose, 80 mM NaCl, 75 mM KCl, 25 mM Hepes, pH = 7.4). Cells were treated with the vehicle (0.5% DMSO) and the metal complexes at their respective $IC_{50}$ values for 1 h. Afterwards, 2 μM of TMRM (tetramethylrhodamine methyl ester) was added and cells protected from light were incubated at room temperature for 15 min. Then, cells were washed twice with PBS and fluorescence was measured at $\lambda_{em}$ = 535 nm with $\lambda_{exc}$ = 590 nm in a microplate reader (Cytation 5 Cell Imaging Multi-Mode Reader -Biotek Instruments, USA). The fluorescence intensity of each well was corrected by the corresponding number of cells. Two independent experiments with 4 replicates per treatment were performed.

### 7) Cell Cycle Arrest

A549 cells ($1.5 \times 10^5$ per well) were seeded in 6 well plates. Cells were treated with each complex at the corresponding $IC_{50}$ value. Cells without any treatment and vehicle-treated cells (0.5% DMSO) were used as control. After 24 h of treatment, cells were harvested and centrifuged, resuspended in cold PBS and fixed in 70% EtOH overnight at 4 °C. Then, samples were treated with 0.1 mg/mL PI, 0.1 mM EDTA and 0.1% Triton- × 100 in PBS to permeabilize and stain cells, and with RNAse (2 mg/mL) for 30 min in ice and protected from light. Finally, cells were analyzed using the NovoCyte Flow cytometer (ACEA Biosciences, Inc., USA). Cell cycle distribution was evaluated by NovoExpress 1.4.0 Software. Two replicates were included and two independent experiments were performed.

### 8) Apoptosis Detection by Flow cytometry

Apoptosis was evaluated by an Annexin V:FITC Assay Kit (Biorad) according to the manufacturer's instructions. Data were collected in a NovoCyte Flow cytometer (ACEA Biosciences, Inc., USA). 10,000 events were counted and analyzed by NovoExpress 1.4.0 Software. Two

replicates and two independent experiments were performed.

*Statistical Analysis*. All the results are expressed as the mean with the standard deviation. Statistical analysis was performed by ANOVA with Dunnet's Test for multiple comparison with the software GraphPad Prism 6.

### 9) Antibacterial activity

Four different strains of pathogenic bacteria, i.e. *E. faecium* CECT 5253 (vancomycin resistant, Gram positive bacteria), *S. aureus* CECT 5190 (methicillin resistant, Gram positive bacteria), *A. baumannii* ATCC 17978 (Gram negative bacteria) and *P. aeruginosa* PAO1 (Gram negative bacteria) were employed. Bacterial strains were maintained as previously described [62]. To test the antibacterial activity, the broth microdilution plate method according to CLSI criteria against ESKAPE (*Enteroccocus faecium, Staphylococcus aureus, Klebsiella pneumoniae, Acinetobacter baumannii, Pseudomonas aeruginosa*, and *Enterobacter cloacae*) pathogens was employed [63]. The reported Minimum Inhibitory concentrations (MIC) are the mean values from at least two independent experiments with three replicates.

### 10) Native PAGE electrophoresis of BSA

Native polyacrylamide gel electrophoresis (PAGE) of BSA was performed as previously described [64]. Briefly, BSA was incubated overnight with different concentrations of **13-Ag** and **14-Au** in sodium cacodylate buffer (2.5 mM), pH = 7, at 37 °C. As vehicle control, BSA incubated with 0.5% DMSO was included. After incubation, samples were diluted 1:1 *v*/v with loading buffer (0.01% bromophenol blue and 20% glycerol in Tris HCl buffer: 0.5 M, pH 6.8). Then, 10 μL of each solution was loaded onto a 10% polyacrylamide gel. Electrophoresis was run in native PAGE buffer (250 mM Tris Base, 1.92 M glycine, pH = 8.3) at 6.6 V/cm for 3.5 h and at 4 °C to avoid BSA thermal denaturation. Afterwards, the gel was stained with Coomassie brilliant blue R-250 and visualized in a Gel Doc XR+ Imaging System (Bio Rad).

### 11) DFT calculations

The ground-state structures were optimized using the range-separated hybrid wB97X DFT functional [65] in combination with Ahlrichs' split-valence-polarized basis set, with relativistic ECPs for Ag and Au [66]. The C-PCM implicit solvation model was added to ωB97X calculations, considering water as continuous medium [67]. The stationary points were characterized by IR simulations (harmonic approximation), from which zero-point vibrational energies and thermal corrections ($T = 25$ °C) were obtained. The software used was Gaussian 09 [68]. Cartesian coordinates of the DFT-optimized structures are collected in a separated .xyz file.

## Author contributions

conceptualization, B.G. and F.M.; methodology, G.B., N.B., G.P., B.G. and F.M.; validation, G.B., N.B., G.P., B.G. and F.M.; formal analysis, G. B., N.B., M.B., G.P., B.G. and F.M.; investigation, G.B., N.B., M.B. and V. C.; data curation, G.B., N.B., M.B., G.P., B.G. and F.M.; writing—original draft preparation, N.B., B.G. and F.M.; writing—review and editing, N. B., G.P., B.G. and F.M.; supervision, G.P., B.G. and F.M.; funding acquisition, N.B., G.P., B.G. and F.M.

## Declaration of Competing Interest

The authors declare that they have no known competing financial interests or personal relationships that could have appeared to influence the work reported in this paper.

## Acknowledgements

The authors gratefully acknowledge the financial support by La Caixa Foundation (LCF/PR/PR12/11070003), Consejería de Educación-Junta de Castilla y León-FEDER Funds (BU305P18), Ministerio de Ciencia, Innovación y Universidades (RTI2018-102040-B-100) and the University of Pisa (PRA_2020_39). We are indebted to Marta Mansilla and Tania Gil (Universidad de Burgos) for the technical support.

## Appendix A. Supplementary data

Figs S1-S23: IR spectra; Figs. S24-S35: NMR spectra. Fig. S36: BSA Native PAGE. Supplementary data to this article can be found online at [https://doi.org/10.1016/j.jinorgbio.2021.111667].

## References

[1] R.L. Siegel, K.D. Miller, A. Jemal, Cancer statistics, 2019, CA Cancer J. Clin. Densitom. 69 (2019) 7–34.

[2] (a) R. Oun, Y.E. Moussa, N.J. Wheate, The side effects of platinum-based chemotherapy drugs: a review for chemists, Dalton Trans. 47 (2018) 6645–6653;
(b) Z.H. Siddik, Cisplatin: mode of cytotoxic action and molecular basis of resistance, Oncogene 22 (2003) 7265–7279;
(c) M.G. Apps, E.H.Y. Choi, N.J. Wheate, The state-of-play and future of platinum drugs, Endocr. Relat. Cancer 22 (2015) R219–R233.

[3] (a) B.S. Murray, P.J. Dyson, Recent progress in the development of organometallics for the treatment of cancer, Curr. Opin. Chem. Biol. 56 (2020) 28–34;
(b) P. Štarha, Z. Trávníček, Non-platinum complexes containing releasable biologically active ligands, Coord. Chem. Rev. 395 (2019) 130–145;
(c) M. Marloye, G. Berger, M. Gelbcke, F. Dufrasne, A survey of the mechanisms of action of anticancer transition metal complexes, Future Med. Chem. 8 (2016) 2263–2286;
(d) T. Lazarević, A. Rilak, Ž.D. Bugarčić, Platinum, palladium, gold and ruthenium complexes as anticancer agents: current clinical uses, cytotoxicity studies and future perspectives, Eur. J. Med. Chem. 142 (2017) 8–31.

[4] (a) E.J. Anthony, E.M. Bolitho, H.E. Bridgewater, O.W.L. Carter, J.M. Donnelly, C. Imberti, E.C. Lant, F. Lermyte, R.J. Needham, M. Palau, P.J. Sadler, H. Shi, F.-X. Wang, W.-Y. Zhang, Z. Zhang, Metallodrugs are unique: opportunities and challenges of discovery and development, Chem. Sci. 11 (2020) 12888–12917;
(b) E. Boros, P.J. Dyson, G. Gasser, Classification of metal-based drugs according to their mechanisms of action, Chem 6 (2020) 41–60.

[5] (a) G. Bresciani, L. Biancalana, G. Pampaloni, F. Marchetti, Recent advances in the chemistry of metal carbamates, Molecules 25 (2020) 3603;
(b) D. Belli Dell'Amico, F. Calderazzo, L. Labella, F. Marchetti, G. Pampaloni, Converting carbon dioxide into carbamato derivatives, Chem. Rev. 103 (2003) 3857–3898.

[6] (a) G. Bresciani, M. Bortoluzzi, S. Zacchini, A. Gabbani, F. Pineider, F. Marchetti, G. Pampaloni, Synthesis and structural characterization of non-homoleptic carbamato complexes of V(V) and W(VI) and their facile implantation onto silica surfaces, Eur. J. Inorg. Chem. 1176–1184 (2018);
(b) M. Bortoluzzi, G. Bresciani, F. Marchetti, G. Pampaloni, S. Zacchini, Synthesis and structural characterization of mixed halide–N,N-diethylcarbamates of group 4 metals, including a case of unusual tetrahydrofuran activation, New J. Chem. 41 (2017) 1781–1789.

[7] (a) G. Bresciani, M. Bortoluzzi, F. Marchetti, G. Pampaloni, Iron(III) N,N-dialkylcarbamate-catalyzed formation of cyclic carbonates from $CO_2$ and epoxides under ambient conditions by dynamic $CO_2$ trapping as carbamato ligands, ChemSusChem 11 (2018) 2737–2743;
(b) G. Bresciani, F. Marchetti, G. Rizzi, A. Gabbani, F. Pineider, G. Pampaloni, Metal N,N-dialkylcarbamates as easily available catalytic precursors for the carbon dioxide/propylene oxide coupling under ambient conditions, J. $CO_2$ Util. 28 (2018) 168–173.

[8] D. Belli Dell'Amico, F. Calderazzo, U. Englert, L. Labella, F. Marchetti, M. Specos, N. New, N-diisopropylcarbamato complexes of ruthenium(II) as catalytic precursors for olefin hydrogenation, Eur. J. Inorg. Chem. 19 (2004) 3938–3945.

[9] (a) T. Babu, A. Sarkar, S. Karmakar, C. Schmidt, D. Gibson, Multiaction Pt(IV) carbamate complexes can codeliver Pt(II) drugs and amine containing bioactive molecules, Inorg. Chem. 59 (2020) 5182–5193;
(b) J. Karges, T. Yempala, M. Tharaud, D. Gibson, G. Gasser, A multi-action and multi-target RuII–PtIV conjugate combining cancer-activated chemotherapy and photodynamic therapy to overcome drug resistant cancers, Angew. Chem. Int. Ed. 59 (2020) 7069–7075.

[10] See also, N. Singh, A. Gupta, P. Prasad, P. Mahawar, S. Gupta, P.K. Sasmal, Iridium-triggered allylcarbamate uncaging in living cells, Inorg. Chem. 60 (2021) 12644–12650.

[11] S. Chen, H. Yao, Q. Zhou, M.-K. Tse, Y.F. Gunawan, G. Zhu, Stability, reduction, and cytotoxicity of platinum(IV) anticancer prodrugs bearing carbamate axial ligands: comparison with their carboxylate analogues, Inorg. Chem. 59 (2020) 11676–11687.

[12] A.K. Ghosh, M. Brindisi, Organic carbamates in drug design and medicinal chemistry, J. Med. Chem. 58 (2015) 2895–2940.
[13] G. Gasser, I. Ott, N. Metzler-Nolte, Organometallic anticancer compounds, J. Med. Chem. 54 (2011) 3–25.
[14] E.Y. Tshuva, D. Peri, Modern cytotoxic titanium(IV) complexes; insights on the enigmatic involvement of hydrolysis, Coord. Chem. Rev. 253 (2009) 2098–2115.
[15] T.-C. Ting, M.-Y. Chang, T.-Y. Hsu, W.-P. Wang, Y.-J. Hsieh, C.-J. Chang, Vanadocene dichloride inhibits cell proliferation by targeting, Aurora B Metall. 10 (2018) 1099–1106.
[16] D. Sanna, V. Ugone, G. Micera, T. Pivetta, E. Valletta, E. Garribba, Speciation of the potential antitumor agent vanadocene dichloride in the blood plasma and model systems, Inorg. Chem. 54 (2015) 8237–8250.
[17] J. Vinklárek, H. Hurychová, J. Honzíček, L. Šebestová, Z. Padělková, M. Řezáčová, Can substitution of chlorides enhance the cytotoxicity of vanadocene dichloride? Eur. J. Inorg. Chem. 2665-2672 (2013).
[18] A. Machalkova, L. Melounkova, J. Vinklarek, I. Cisarova, J. Honzicek, Synthesis, characterization and cytotoxic activity of vanadocene dithiocarbamate complexes, Inorg. Chim. Acta 485 (2019) 125–130.
[19] F. Marchetti, G. Pampaloni, Interaction of niobium and tantalum pentahalides with O-donors: coordination chemistry and activation reactions, Chem. Commun. 48 (2012) 635–653.
[20] D. Zhang, Z. Liang, S. Xie, P. Ma, C. Zhang, J. Wang, J. Niu, A new $Nb_{28}$ cluster based on tungstophosphate $[\{Nb_4O_6(OH)_4\}\{Nb_6P_2W_{12}O_{61}\}_4]^{36-}$, Inorg. Chem. 53 (2014) 9917–9922.
[21] A. Eskandaria, K. Suntharalingam, A reactive oxygen species-generating, cancer stem cell-potent manganese(II) complex and its encapsulation into polymeric nanoparticles, Chem. Sci. 10 (2019) 7792–7800.
[22] U. Basu, M. Roy, A.R. Chakravarty, Recent advances in the chemistry of iron-based chemotherapeutic agents, Coord. Chem. Rev. 417 (2020), 213339.
[23] (a) S. Thota, D.A. Rodrigues, D.C. Crans, E.J. Barreiro, Ru(II) compounds: next-generation anticancer metallotherapeutics? J. Med. Chem. 61 (14) (2018) 5805–5821;
(b) A.A. Nazarov, C.G. Hartinger, P.J. Dyson, Opening the lid on piano-stool complexes: an account of ruthenium(II)–arene complexes with medicinal applications, J. Organomet. Chem. 751 (2014) 251–260.
[24] P. Mandal, B. Kumar Kundu, K. Vyas, V. Sabu, A. Helen, S. Singh Dhankhar, C. M. Nagaraja, D. Bhattacherjee, K. Pada Bhabak, S. Mukhopadhyay, Ruthenium(II) arene NSAID complexes: inhibition of cyclooxygenase and antiproliferative activity against cancer cell lines, Dalton Trans. 47 (2018) 517–527.
[25] M. Melchart, A. Habtemariam, S. Parsons, S.A. Moggach, P.J. Sadler, Ruthenium (II) arene complexes containing four- and five-membered monoanionic O,O-chelate rings, Inorg. Chim. Acta 359 (2006) 3020–3028.
[26] (a) B. Bertrand, A. Casini, A golden future in medicinal inorganic chemistry: the promise of anticancer gold organometallic compounds, Dalton Trans. 43 (2014) 4209–4219;
(b) I. Ott, On the medicinal chemistry of gold complexes as anticancer drugs, Coord. Chem. Rev. 253 (2009) 1670–1681.
[27] M.P. Chrysouli, C.N. Banti, N. Kourkoumelis, N. Panayiotou, G.S. Markopoulos, A. J. Tasiopoulos, S.K. Hadjikakou, Chloro(triphenylphosphine)gold(I) a forefront reagent in gold chemistry as apoptotic agent for cancer cells, J. Inorg. Biochem. 179 (2018) 107–120.
[28] J.C. Lima, L. Rodriguez, Phosphine-gold(I) compounds as anticancer agents: general description and mechanisms of action, Anti Cancer Agents Med. Chem. 11 (2011) 921–928.
[29] A.K. Renfrew, N.S. Bryce, T. Hambley, Cobalt(III) chaperone complexes of curcumin: photoreduction, cellular accumulation and light-selective toxicity towards tumour cells, Chem. Eur. J. 21 (2015) 15224–15234.
[30] C. Santini, M. Pellei, V. Gandin, M. Porchia, F. Tisato, C. Marzano, Advances in copper complexes as anticancer agents, Chem. Rev. 114 (2014) 815–862.
[31] S. Medici, M. Peana, G. Crisponi, V.M. Nurchi, J.I. Lachowicz, M. Remelli, M. A. Zoroddu, Silver coordination compounds: a new horizon in medicine, Coord. Chem. Rev. 327–328 (2016) 349–359.
[32] S.K. Hadjikakou, N. Hadjiliadis, Antiproliferative and anti-tumor activity of organotin compounds, Coord. Chem. Rev. 253 (2009) 235–249.
[33] M. Bortoluzzi, F. Ghini, M. Hayatifar, F. Marchetti, G. Pampaloni, S. Zacchini, Oxido- and sulfidoniobium(V) N,N-diethylcarbamates: synthesis, characterization and DFT study, Eur. J. Inorg. Chem. (2013) 3112–3118.
[34] D. Belli Dell'Amico, L. Labella, F. Marchetti, P. Mastrorilli, S. Samaritani, S. Todisco, Oxidation by dioxygen of manganese(II) and iron(II) complexes, Polyhedron 65 (2013) 275–281.
[35] L. Biancalana, G. Pampaloni, S. Zacchini, F. Marchetti, Synthesis, characterization and behavior in water/DMSO solution of Ru(II) arene complexes with bioactive carboxylates, J. Organomet. Chem. 869 (2018) 201–211.
[36] L. Melounková, A. Machálková, R. Havelek, J. Honzíček, M. Řezáčová, I. Císařová, E. Peterová, J. Vinklárek, Vanadocene complexes bearing N,N'-chelating ligands: synthesis, structures and in vitro cytotoxic studies on the A549 lung adenocarcinoma cell line, J. Inorg. Biochem. 195 (2019) 182–193.
[37] (a) A. Gutierrez, I. Marzo, C. Cativiela, A. Laguna, M.C. Gimeno, Highly cytotoxic bioconjugated gold(I) complexes with cysteine- containing dipeptides, Chem. Eur. J. 21 (2015) 11088–11095;
(b) A. Gutiérrez, L. Gracia-Fleta, I. Marzo, C. Cativiela, A. Laguna, M.C. Gimeno, Gold(I) thiolates containing amino acid moieties. Cytotoxicity and structure–activity relationship studies, Dalton Trans. 43 (2014) 17054–17066;
(c) P. Štarha, Z. Trávníček, B. Drahoš, Z. Dvorák, Int. J. Mol. Sci. 17 (2016) 2084.
[38] P. Chrysouli, C.N. Banti, N. Kourkoumelis, N. Panayiotou, G.S. Markopoulos, A. J. Tasiopoulos, S.K. Hadjikakou, Chloro(triphenylphosphine)gold(I) a forefront reagent in gold chemistry as apoptotic agent for cancer cells, J. Inorg. Biochem. 179 (2018) 107–120.
[39] (a) C. Nguyen, S. Pandey, Exploiting mitochondrial vulnerabilities to trigger apoptosis selectively in cancer cells, Cancers 11 (2019) 916;
(b) L. Galluzzi, O. Kepp, M.G. Vander Heiden, G. Kroemer, Metabolic targets for cancer therapy, Nat. Rev. Drug Discov. 12 (2013) 829–846;
(c) R.J. DeBerardinis, N.S. Chandel, We need to talk about the Warburg effect, Nat. Metab. 2 (2020) 127–129.
[40] T. Zou, C.T. Lum, C.-N. Lok, J.-J. Zhang, C.-M. Che, Chemical biology of anticancer gold(III) and gold(I) complexes, Chem. Soc. Rev. 44 (2015) 8786–8801.
[41] S. Creed, M. McKenzie, Measurement of mitochondrial membrane potential with the fluorescent dye tetramethylrhodamine methyl ester (TMRM), in: M. Haznadar (Ed.), Cancer Metabolism. Methods in Molecular Biology 1928, Humana Press, New York, NY, 2019, https://doi.org/10.1007/978-1-4939-9027-6_5.
[42] A.V. Snezhkina, A.V. Kudryavtseva, O.L. Kardymon, M.V. Savvateeva, N. V. Melnikova, G.S. Krasnov, A.A. Dmitriev, ROS generation and antioxidant defense systems in normal and malignant cells, Oxidative Med. Cell. Longev. 6175804 (2019), https://doi.org/10.1155/2019/6175804.
[43] S. Rhee, T.-S. Chang, W. Jeong, D. Kang, Methods for detection and measurement of hydrogen peroxide inside and outside of cells, Mol. Cell 29 (2010) 539–549.
[44] A. Wojtala, M. Bonora, D. Malinska, P. Pinton, J. Duszynski, M.R. Wieckowski, Methods to monitor ROS production by fluorescence microscopy and fluorometry, Methods Enzymol. 542 (2014) 243–262.
[45] B. Perillo, M. Di Donato, A. Pezone, et al., ROS in cancer therapy: the bright side of the moon, Exp. Mol. Med. 52 (2020) 192–203.
[46] (a) A. Frei, J. Zuegg, A.G. Elliott, M. Baker, S. Braese, C. Brown, F. Chen, C. G. Dowson, G. Dujardin, N. Jung, A. Paden King, A.M. Mansour, M. Massi, J. Moat, H.A. Mohamed, A.K. Renfrew, P.J. Rutledge, P.J. Sadler, M.H. Todd, C.E. Willans, J.J. Wilson, M.A. Cooper, M.A.T. Blaskovich, Metal complexes as a promising source for new antibiotics, Chem. Sci. 11 (2020) 2627–2639;
(b) S. Medici, M. Peana, V.M. Nurchi, M.A. Zoroddu, Medical uses of silver: history, myths, and scientific evidence, J. Med. Chem. 62 (2019) 5923–5943.
[47] İ. Özdemir, A. Denizci, H.T. Öztürk, B. Cetinkaya, Synthetic and antimicrobial studies on new gold(I) complexes of imidazolidin-2-ylidenes, Appl. Organomet. Chem. 18 (2004) 318–322.
[48] F. Calderazzo, S. Ianelli, G. Pampaloni, G. Pelizzi, M. Sperrle, Synthesis of N,N-dialkylcarbamato complexes of Group 4 metals (Ti, Zr, Hf) by the metal chloride-$NHR_2$-$CO_2$ system (R = Et or $Pr^i$): crystal and molecular structure of $[Hf(O_2CNPr^i_2)_4]$, J. Chem. Soc. Dalton Trans. (1991) 693–698.
[49] P.B. Arimondo, F. Calderazzo, U. Englert, C. Maichle-Mössmer, G. Pampaloni, J. Strähle, Preparation and characterization of dialkylcarbamato derivatives of niobium and tantalum, J. Chem. Soc. Dalton Trans. (1996) 311–319.
[50] D. Belli, D. Amico, D. Boschi, F. Calderazzo, S. Ianelli, L. Labella, F. Marchetti, G. Pelizzi, E. Guy, F. Quadrelli, N, N-Dialkylcarbamato μ-oxo derivatives of iron (III), Inorg. Chim. Acta 302 (2000) 882–891.
[51] D. Belli Dell'Amico, F. Calderazzo, L. Labella, F. Marchetti, E. Sbrana, Organometallic complexes of ruthenium(II) with N,N-dialkylcarbamato as the supporting ligand, J. Organomet. Chem. 651 (2002) 52–59.
[52] D. Belli Dell'Amico, F. Calderazzo, B. Giovannitti, G. Pelizzi, NN-Dialkylcarbamato-complexes of cobalt(II), J. Chem. Soc. Dalton Trans. (1984) 647–652.
[53] E. Agostinelli, D. Belli Dell'Amico, F. Calderazzo, D. Fiorani, G. Pelizzi, Synthesis, properties and crystal and molecular strucrture of $Cu_2(O_2CNEt_2)_4$ $2NHEt_2$, Gazz, Chim. Ital. 188 (1988) 729–740.
[54] R. Alessio, D. Belli Dell'Amico, F. Calderazzo, U. Englert, A. Guarini, L. Labella, P. Strasser, N,N-dialkylcarbamato complexes of the $d^{10}$ cations of copper, silver, and gold, Helv. Chim. Acta 81 (1998) 219–230.
[55] L. Abis, D. Belli Dell'Amico, F. Calderazzo, R. Caminiti, F. Garbassi, S. Ianelli, G. Pelizzi, P. Robino, A. Tomei, N,N-dialkylcarbamato complexes as precursors for the chemical implantation of metal cations on a silica support. Part I. Tin, J. Mol. Cat. A; Chem. 108 (1996) L113–L117.
[56] F. Menges, Spectragryph - Optical Spectroscopy Software, Version 1.2.5, @ 2016–2017, http://www.effemm2.de/spectragryph.
[57] G.R. Fulmer, A.J.M. Miller, N.H. Sherden, H.E. Gottlieb, A. Nudelman, B.M. Stoltz, J.E. Bercaw, K.I. Goldberg, NMR chemical shifts of trace impurities: common laboratory solvents, organics, and gases in deuterated solvents relevant to the organometallic chemist, Organometallics 29 (2010) 2176–2179.
[58] R.K. Harris, E.D. Becker, S.M. Cabral De Menezes, R. Goodfellow, P. Granger, NMR nomenclature. Nuclear spin properties and conventions for chemical shifts(IUPAC Recommendations 2001), Pure Appl. Chem. 73 (2001) 1795–1818.
[59] $^1$H NMR spectrum of $[NH_2Et_2]Cl$ in (DMSO-$d_6$ + $D_2O$): δ/ppm = 4.00 (br, $NH_2$); 2.86 (q, $^3J_{HH}$ = 7.3 Hz, 2H, $CH_2$); 1.14 (t, $^3J_{HH}$ = 7.3 Hz, 3H, Me), 2021.
[60] (a) C.C. Westcott, pH Measurements, Academic Press, New York, 1978;
(b) (Calculated by the formula pD = pH* + 0.4, where pH* is the value measured for $H_2O$-calibrated pHmeter) A.K. Covington, M. Paabo, R.A. Robinson, R.G. Bates, Use of the glass electrode in deuterium oxide and the relation between the standardized pD (paD) scale and the operational pH in heavy water, Anal. Chem. 40 (1968) 700–706.
[61] E. Zanda, N. Busto, L. Biancalana, S. Zacchini, T. Biver, B. Garcia, F. Marchetti, Anticancer and antibacterial potential of robust ruthenium(II) arene complexes regulated by choice of α-diimine and halide ligands, Chem.-Biol. Interact. 344 (2021), 109522.
[62] E. Ortega, C. Pérez-Arnaiz, V. Rodríguez, C. Janiak, N. Busto, B. García, J. Ruiz, A 2-(benzothiazol-2-yl)-phenolato platinum(II) complex as potential photosensitizer for combating bacterial infections in lung cancer chemotherapy, Eur. J. Med. Chem. 222 (2021), 113600.

[63] Clinical and Laboratory Standards Institute, Performance Standards for Antimicrobial Susceptibility Testing: 17th Informational Supplement M07-A9, Clinical and Laboratory Standards Institute, Wayne, PA, 2012.

[64] M. Vaquero, N. Busto, N. Fernández-Pampín, G. Espino, B. García, Appended aromatic moieties determine the cytotoxicity of neutral cyclometalated platinum (II) complexes derived from 2-(2-Pyridyl)benzimidazole, Inorg. Chem. 59 (2020) 4961–4971.

[65] (a) Y. Minenkov, Å. Singstad, G. Occhipinti, V.R. Jensen, The accuracy of DFT-optimized geometries of functional transition metal compounds: a validation study of catalysts for olefin metathesis and other reactions in the homogeneous phase, Dalton Trans. 41 (2012) 5526–5541;
(b) J.-D. Chai, M. Head-Gordon, Long-range corrected hybrid density functionals with damped atom-atom dispersion corrections, Phys. Chem. Chem. Phys. 10 (2008) 6615–6620;
(c) I.C. Gerber, J.G. Ángyán, Hybrid functional with separated range, Chem. Phys. Lett. 415 (2005) 100–105.

[66] (a) F. Weigend, R. Ahlrichs, Balanced basis sets of split valence, triple zeta valence and quadruple zeta valence quality for H to Rn: design and assessment of accuracy, Phys. Chem. Chem. Phys. 7 (2005) 3297–3305;
(b) D. Andrae, U. Häußermann, M. Dolg, H. Stoll, H. Preuß, Energy-adjusted ab initio pseudopotentials for the second and third row transition elements, Theor. Chim. Acta 77 (1990) 123–141.

[67] (a) M. Cossi, N. Rega, G. Scalmani, V. Barone, V. Energies, Structures, and electronic properties of molecules in solution with the C-PCM solvation model, J. Comput. Chem. 24 (2003) 669–681;
(b) V. Barone, M. Cossi, Quantum calculation of molecular energies and energy gradients in solution by a conductor solvent model, J. Phys. Chem. A 102 (1998) 1995–2001.

[68] M.J. Frisch, G.W. Trucks, H.B. Schlegel, G.E. Scuseria, M.A. Robb, J.R. Cheeseman, G. Scalmani, V. Barone, B. Mennucci, G.A. Petersson, H. Nakatsuji, M. Caricato, X. Li, H.P. Hratchian, A.F. Izmaylov, J. Bloino, G. Zheng, J.L. Sonnenberg, M. Hada, M. Ehara, K. Toyota, R. Fukuda, J. Hasegawa, M. Ishida, T. Nakajima, Y. Honda, O. Kitao, H. Nakai, T. Vreven, J.A. Montgomery Jr., J.E. Peralta, F. Ogliaro, M. Bearpark, J.J. Heyd, E. Brothers, K.N. Kudin, V.N. Staroverov, R. Kobayashi, J. Normand, K. Raghavachari, A. Rendell, J.C. Burant, S.S. Iyengar, J. Tomasi, M. Cossi, N. Rega, J.M. Millam, M. Klene, J.E. Knox, J.B. Cross, V. Bakken, C. Adamo, J. Jaramillo, R. Gomperts, R.E. Stratmann, O. Yazyev, A.J. Austin, R. Cammi, C. Pomelli, J.W. Ochterski, R.L. Martin, K. Morokuma, V.G. Zakrzewski, G.A. Voth, P. Salvador, J.J. Dannenberg, S. Dapprich, A.D. Daniels, Ö. Farkas, J. B. Foresman, J.V. Ortiz, J. Cioslowski, D.J. Fox, Gaussian 09, Revision C.01, Gaussian Inc, Wallingford, CT, 2010.